Numerical modelling of lateral load-deformation curves for timber poles embedded in stiff clay

La modélisation numérique des courbes charge-déformation latérale pour poteaux bois incorporés dans les argiles raides

Michael Pender, *Department of Civil and Environmental Engineering, University of Auckland, New Zealand. m.pender@auckland.ac.nz*
Peter Rodgers, *Mercury Civil Design Ltd., peter@mbcd.co.nz*

* Presenting Author Name: Michael Pender
* Corresponding Author: Michael Pender (Member of ISSMGE)

ABSTRACT: We have done field testing of prototype scale laterally loaded timber poles in Auckland residual clay. A frequent application of these foundations around Auckland is to pole retaining walls. The poles are embedded in unreinforced concrete in pre-bored holes. The poles of *pinus radiata* were 250mm in diameter and the concrete embedment 450 mm in diameter. The depth of embedment ranged between 2 and 5 embedment diameters. The lateral load was applied between 0.5 and 1 m above the ground surface. To date our interpretation of the field test data has concentrated on each end of the test results: initial stiffness and ultimate lateral capacity. Between these two limits there lies a curved transition which, in the past, we have modelled using a hyperbolic curve. We used the data obtained from the field testing to derive design relationships for the capacity of laterally loaded poles; this work is presented in Pender and Rodgers (2016). The purpose of this paper is to explore the nature of the curved transition using finite element software which can handle 3D nonlinear soil behavior, OpenSeesPL (Lu et al. (2010)).

RÉSUMÉ : Nous avons fait l'essai sur le terrain d'échelle prototype poteaux bois chargés latéralement dans l'argile résiduelle d'Auckland. Une application fréquente de ces fondations autour d'Auckland est à l'autre des murs de soutènement. Les Polonais sont intégrés dans béton non armé en pré-percée de trous. Les poteaux de Pinus radiata sont 250mm de diamètre et de l'encastrement béton 450 mm de diamètre. La profondeur de l'encastrement variait entre 2 et 5 diamètres d'encastrement. La charge latérale a été appliquée entre 0,5 et 1 m au-dessus de la surface du sol. À ce jour notre interprétation des données d'essai sur le terrain s'est concentré sur chaque extrémité des résultats du test : rigidité initiale et la capacité latérale ultime. Entre ces deux limites, il y a une courbe de transition qui nous avons modélisé à l'aide d'une courbe hyperbolique. Nous avons utilisé les données obtenues à partir de l'essai sur le terrain pour établir des relations de conception pour la capacité des pôles chargés latéralement ; ce travail est présenté de Pender et Rodgers (2016). Le but de cet article est d'explorer la nature de la transition à l'aide du logiciel d'éléments finis qui peuvent gérer le comportement des sols non linéaire 3D, OpenSeesPL (Lu et al. (2010)).

KEYWORDS: Timber pole, stiff clay, lateral displacement curve, 3D nonlinear finite element modelling, undrained shear strength.

1 INTRODUCTION

We have done field testing of prototype scale laterally loaded timber poles in Auckland residual clay. A frequent application of these foundations around Auckland is to pole retaining walls. The poles are embedded in unreinforced concrete in pre-bored holes. The poles of *pinus radiata* were 250mm in diameter and the concrete embedment is 450 mm in diameter. The depth of embedment is in the range of 3 to 5 embedment diameters. In retaining wall design the lateral load is applied above the ground surface, typically about 1 m.

We use the term pole, rather than pile, because the concrete embedment ensures that the system behaves in an approximately rigid manner as distinct from a long pile which is flexible.

To check on the actual lateral capacity, field tests were done on poles embedded in Auckland residual clay at a site near Fairview Avenue in Albany (north of Auckland city in New Zealand). The top half metre or so was scalped from the site (to a depth a little below the topsoil) and a working platform prepared. Thirteen poles installed were 0.25 m SED (small end diameter) sections of *pinus radiata* and concreted (with no reinforcing) into 0.45m diameter auger holes. The 28 day crushing strength of the embedment concrete was 26 MPa. The embedment depths varied as did the height above the ground surface at which the lateral load was applied.

We used the data obtained from the field testing to derive design relationships for the capacity of laterally loaded poles. For poles with shallow embedment depths we were able to improve on the short pole capacity given by Broms (1964); work presented in Pender and Rodgers (2016).

In this paper we report on preliminary finite element work to investigate the lateral load behavior of timber poles embedded in the stiff cohesive soil with a view to understanding better the interaction between the embedded part of the pole and the surrounding soil. An additional point of interest is the effect of the interface properties between the embedded pole shaft and the surrounding soil and, furthermore, how the values for the soil properties used in the finite element analysis relate to the values obtained during our site investigation.

2 SOIL PROPERTIES

The residual clay from the part of Auckland where the testing was done has tan brown colour with grey streaking and, to the naked eye, is a uniform material although it has been shown that there may be macro-voids present in the material (Pender et al. 2009). The Atterberg limits for the clay are: PL about 33%,

Figure 1. Ground surface around a pole shaft near the end of the lateral loading. Note the embedment concrete and the gap which has opened behind.

LL about 74%, and the natural water contents are about 35 to 40%. The effective stress constant volume friction angle of the clay is about 25 degrees.

At the location of each pole a shear strength profile was obtained with a Geonor H-60 hand vane having a 20 mm diameter and 40 mm tall vane. A small diameter hand auger was used to assist the vane shear strength measurements. The vane shear strength values obtained were approximately constant over the depth of the pole embedment at about 90 kPa.

Figure 1 shows the ground surface near the pole towards the end of one of the lateral load tests – the loading is from the left hand side of the diagram. Some of the instrumentation, the reference beam, the concrete embedment, and the gap that opens between the ground and the embedment concrete are visible.

3 FINITE ELEMENT MODELLING

Three dimensional finite element modelling was used to compare the measured lateral load – ground level lateral deformation responses of the embedded poles. The modelling was done with OpenSeesPL (Lu et al. 2010) which has been developed within the OpenSees framework, (Mazzoni et al. 2009), specifically for calculations involving pile-soil interaction. The pile is vertical but the ground surface does not have to be horizontal, the meshing within the "soil box" is semi-automated so that the element size increases with distance from the pile shaft. Actions can be applied to the pile head, both static and dynamic, earthquake motions can be applied to the base of the finite element mesh, and a range of boundary conditions are available. Eight node and twenty node brick elements are available for the 3D soil discretisation. The software also has the facility to account for nonlinear soil and nonlinear pile behaviour. OpenSeesPL differs from OpenSees in that a graphical user interface is provided for input of model details and post-processing is provided for plotting the output data.

Part of the finite element mesh used for the embedded pole-soil modelling is shown in Figure 2. The dimensions of the mesh block are: length 40 m and width 20 m and depth 5 m; the embedded part of the pole is up to 2 m long. The mesh has 15 elements in the radial direction (closely spaced near to the pile shaft), in the vertical direction there are 16 elements, and in the circumferential direction 16 elements. As can be seen from Figure 2, symmetry means that only half the pole-soil mesh needs to be modelled.

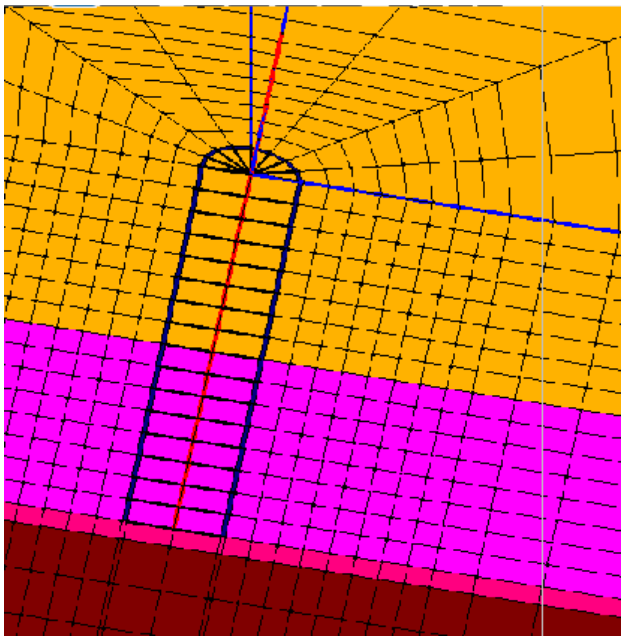

Figure 2. A tilted cross-section through the finite element mesh showing the plane of symmetry and the ground surface. The heavy boundary around the pole is the interface; note also the thin soil layer at the base of the embedment.

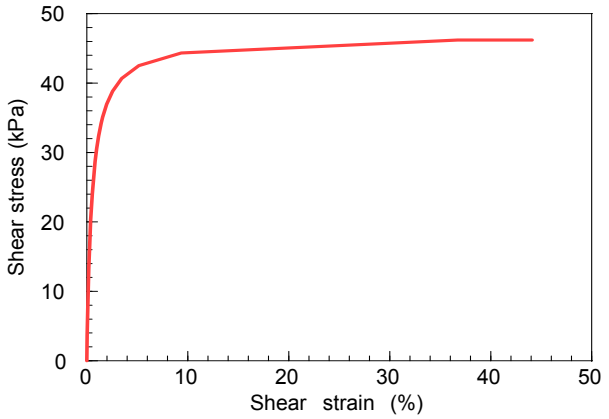

Figure 3. Shear stress – shear strain curve for the stiff clay generated by the Pressure-Independent Multi-yield surface material model in OpenSeesPL.

The pole was assumed to be elastic. Since the pole-concrete is a composite the question of the appropriate value of Young's modulus arises as the timber pole and concrete sleeve were not modelled with separate materials. The Young's modulus of the timber pole is about 12 GPa and for the unreinforced concrete the value is about 22 GPa. The output of the finite element modelling shows that the concrete encased pole is effectively rigid relative to the surrounding soil, so a single Young's modulus value of 12 GPa was used for the composite.

The clay, assumed to be saturated, was modelled with the Pressure Independent Multi-yield surface material in OpenSeesPL. Plastic yielding of the soil is represented with a nested series of conical kinematic yield loci following the ideas of Prevost (1978). The main input parameters are the undrained shear shear strength and shear modulus of the clay. Since undr-

Table 1. Details of lateral load tests on poles 3, 6 and 9.

Pole number*	3	6	9
Embedment depth (m)	1.0	2.0	1.6
Height of load (m)	0.5	0.8	1.0

*The embedment diameter for all poles was 0.45m

ained behavior is modelled, Poisson's ratio for the soil was set to 0.49.

The shear stress – shear strain curve for the undrained behavior of the clay is shown in Figure 3.

4 OUTPUT FROM FINITE ELEMENT MODELLING

The lateral and bottom boundaries are sufficiently remote that they do not influence the results of the analysis, so they are fully fixed. OpenSeesPL has an interface between the pole shaft and the surrounding soil, shown in Figure 2. The best matching between the calculated load-deformation curves and those obtained in the field testing was obtained by making this interface as smooth as possible; sand with a friction angle of 5 degrees worked slightly better than very soft clay. Without this low strength interface the calculated lateral resistance was much larger than that determined in the field testing. Also there is a no-tension cutoff facility for cohesive soil in OpenSeesPL which was mobilised in all the calculations.

Figures 4, 5 and 6 compare the finite element and field measured lateral load deformation curves for three of the poles tested; the pole details are given in Table 1. It is clear that for all three poles the matches between the lateral resistances calculated with OpenSeesPL and those measured in the field testing are good.

Figure 7 has the calculated displacement profiles of the embedded part of pole 6 for increasing lateral loads (the direction of the applied lateral load is towards the right hand side of the figure). The linearity of these profiles confirms the comment made earlier that, relative to the clay, the concrete encased pole acts as a rigid member. Also there is a cross-over at a depth 1.3 to 1.4 m so that above this level the soil reaction is to the left and below it is to the right hand side of the plot.

Figure 8 shows the calculated soil pressure acting against the centreline of the embedded part of the pole, both in front and behind. These plots confirm that the interface between the embedded part of the pole and the clay does not generate tensile resistance.

5 OPERATIONAL SOIL MODULUS AND UNDRAINED SHEAR STRENGTH

Measurements of the shear wave velocity in Auckland residual clay at sites within a few kilometres from the pole lateral load test site gave a small strain shear modulus of about 30 MPa. Allowing for undrained behaviour of saturated soil, this gives a Young's modulus of 90 MPa. However, when this value is used the calculated initial stiffnesses of the load deformation curves are much greater than those indicated in Figures 4, 5 and 6. We have also come to similar conclusions from field testing of shallow foundations on Auckland residual clay. So, to achieve good modelling of the initial linear part of the load deformation curve, we need to use a Young's modulus about one quarter to one third of the value derived from the shear wave velocity. We refer to this reduced value as the *operational soil modulus*.

Having obtained the vane shear strength from our site investigation, we used this value in the initial finite element runs. However, the calculated load-deformation curve was then much higher than the curve obtained from the field tests. We found that if the undrained shear strength in the OpenSeesPL finite element model was set to about half the measured vane shear strength, then an excellent match was achieved between the calculated and measured data points; this is the basis of the plots in Figures 4, 5 and 6. We thus propose that the *operational undrained shear strength* is about half the vane shear strength.

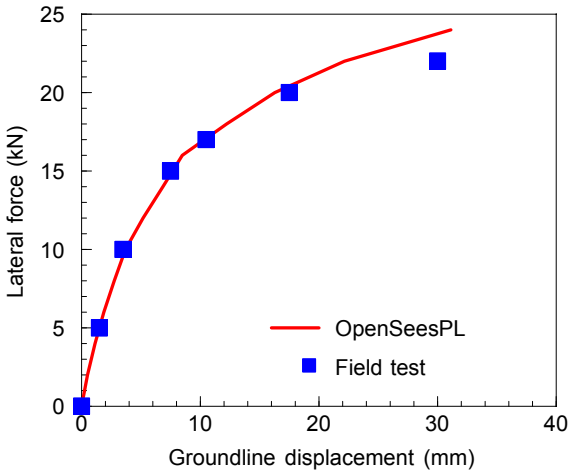

Figure 4. Pole 3: comparison between the OpenSeesPL groundline lateral displacement and the displacements measured in the field tests.

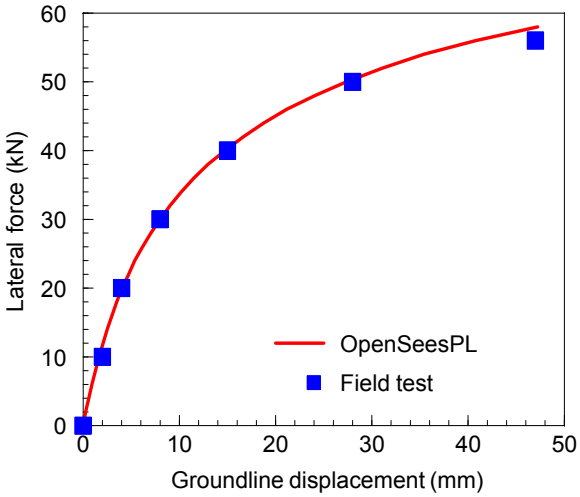

Figure 5. Pole 6: comparison between the OpenSeesPL groundline lateral displacement and the displacements measured in the field tests.

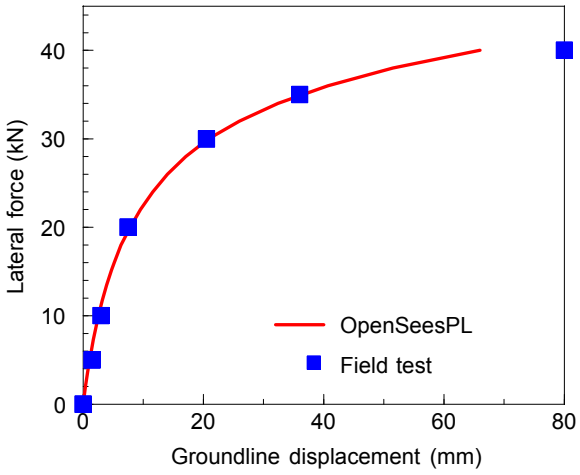

Figure 6. Pole 9: comparison between the OpenSeesPL groundline lateral displacement and the displacements measured in the field tests.

It is one thing to find that a reduced soil modulus is needed to achieve good modelling, but quite another to suggest halving the undrained shear strength of the soil. Initially one might be suspicious of the finite element software or an error in the input. However, this is unlikely as we have achieved successful modelling of laterally loaded behaviour of long piles using OpenSeesPL (Pender et al (2012)). The simplicity of the vane shear strength test belies the fact that there is not one single undrained shear strength value, rather it depends on the mode of shearing (Ohta et al. 1985). There is also the possibility that the assumption of undrained behavioiur is not correct and that, particularly near the ground surface, drained behaviour might have occurred. Again, it is difficult to see how this could account for a factor of two in the shear strength.

On reflection, we think the most likely explanation is that the clay at the sides of the 450 mm diameter augered holes absorbed water from the wet concrete with a consequent reduction in undrained shear strength; a relatively small change in water content would reduce the undrained shear stength substantially. If this is the case there is likely to be a lateralal variation in the water content of the clay adjacent to the concrete embedment with a consequent lateral variation in undrained shear strength; so the above operational undrained shear strength would be an average value for the volume of clay affected by the pole loading.

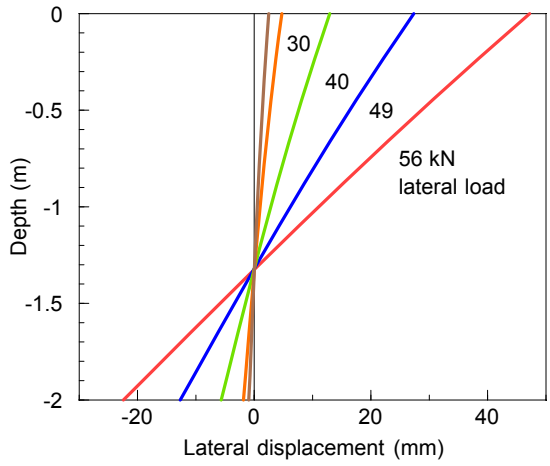

Figure 7. Pole 6: calculated lateral displacement profiles for the embedded part of the pole at increasing lateral loads.

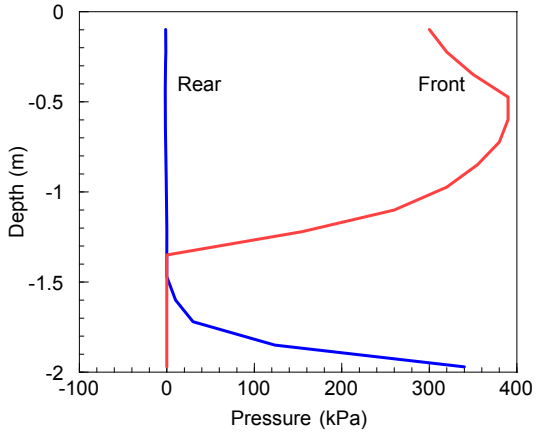

Figure 8. Pole 6, at the maximum lateral load (56kN), calculated centreline lateral soil pressure against the front and rear faces.

6 CONCLUSIONS

Reported herein is a preliminary investigation, using 3D nonlinear finite element analysis, on the measured lateral load-deformation behaviour of timber poles concreted into pre-augered holes in Auckland residual clay.

We conclude that:

- A very good match has been obtained between the field test load-deformation data and the finite element results (Figures 4, 5 and 6).
- The interface between the embedded pole and the surrounding soil must be close to smooth to obtain a good match between finite element calculations and the field data.
- The calculated displaced shape of the embedded pole shaft indicates essentially rigid behaviour with a point of rotation towards the base of the embedded part (Figure 7).
- One face of the embedded part of the pole shaft sustains compressive normal contact stresses, on the other face the normal stresses are close to zero (Figure 8).
- The soil modulus required to give a satisfactory match between the initial linear stiffness of the measured load-deformation curves and those from the finite element results is about one third of the value calculated from the shear wave velocity of the clay.
- The undrained shear strength required to give a satisfactory match between the finite element load-deformation curves and the measured curves is about half the vane shear strength for the clay.

7 REFERENCES

Broms B B. 1964. Lateral resistance of piles in cohesive soils. *Journal of Soil Mechanics and Foundations ASCE*, 90(SM3): 27-63.

Lu, J., Yang, Z., and Elgamal, A. 2010. *OpenSeesPL 3D lateral pile-ground interaction: User's manual.* University of California, San Diego. (https://neesforge.nees.org/projects/OpenSeesPL)

Mazzoni, S., McKenna, F., Scott, M. H., and Fenves, G. L. 2009. *Open system for earthquake engineering simulation user manual*, University of California, Berkeley. (http://opensees.berkeley.edu/)

Ohta, H., Nishihara, A. and Morito, Y. 1985. Undrained stability of Ko consolidated clay. *Proc. 11th ICSMFE,* San Francisco, 613 – 616.

Pender, M. J. and Rodgers, P. 2016. Ultimate lateral capacity of timber poles embedded in clay. *ICE Geotechnical Engineering*, 169 (GE2), 175–186. [http://dx.doi.org/10.1680/jgeen.15.00037].

Pender M. J., Kikkawa, N. and Liu, P. 2009. Macro-void structure and permeability of Auckland residual clay, *Geotechnique* LIX(9): 773-778.

Pender, M J, Wotherspoon, L. M., M.Sa'don, N. and Orense, R. P. 2012. Macro-element for pile head cyclic lateral loading. In: *Advances in Earthquake Geotechnical Engineering*, chapter 5, M. Sakr and A. Ansal editors, Springer, 129-145.

Prevost, J H (1978). Plasticity Theory for Soil Stress-Strain Behavior. *Journal of Engineering Mechanics-ASCE.* 104 (EM5), 1177-1194.